

## Article

# Real-Time Identification of Cyanobacteria Blooms in Lakeshore Zone Using Camera and Semantic Segmentation: A Case Study of Lake Chaohu (Eastern China)

Zhiyong Wang <sup>1</sup>, Chongchang Wang <sup>1,\*</sup>, Yuchen Liu <sup>2</sup>, Jindi Wang <sup>1</sup> and Yinguo Qiu <sup>2,\*</sup><sup>1</sup> School of Surveying, Mapping and Geographical Sciences, Liaoning Technical University, Fuxin 123000, China<sup>2</sup> Key Laboratory of Watershed Geography, Nanjing Institute of Geography and Limnology, Chinese Academy of Sciences, Nanjing 210008, China

\* Correspondence: lgdclxwang@163.com (C.W.); ygqiu@niglas.ac.cn (Y.Q.)

**Abstract:** The surface water in the lakeshore zone is the primary area where cyanobacteria bloom floats intensively. In lake water environment monitoring, it has become pressing to accurately identify the distribution and accumulation coverage area of cyanobacteria blooms in the surface water of the lakeshore zone. This study proposes a real-time and dynamic monitoring technology for cyanobacteria blooms in surface water using a shore-based camera monitoring network. The specific work is as follows: Chaohu Lake, a large eutrophic lake in China, is selected as the research object. The multithreading technology is used to dynamically obtain the hourly video images of 43 cameras around Chaohu Lake. The semantic segmentation method is used to identify the cyanobacteria blooms in the video images, calculate the coverage of cyanobacteria blooms, and draw the spatial distribution map of cyanobacteria blooms in the lakeshore zone of Chaohu Lake. To improve the accuracy of cyanobacteria blooms recognition, we use the ResNet-50 network to integrate three semantic segmentation models, namely FCN, U-net, and DeeplabV3+. By comparing the cyanobacteria blooms results identified by the three methods, it is found that the boundary of the cyanobacteria blooms results identified by DeeplabV3+(ResNet-50) is clear, which is more consistent with the real spatial information of the distribution of cyanobacteria blooms and is more suitable for monitoring the hourly dynamic changes of cyanobacteria blooms in the Chaohu Lake lakeshore zone. The results demonstrated that the time requirement of monitoring cyanobacteria blooms in real time on an hourly basis could be met by utilizing technology that uses multiple threads. The OA (Overall Accuracy), MPA (Mean Pixel Accuracy), IOU (Intersection Over Union) of cyanobacteria blooms, and the IOU of water values of the DeeplabV3+(ResNet-50) were the highest, which were 0.83, 0.82, 0.71, and 0.74, and the RMSE between the predicted and real cyanobacterial blooms coverage of 43 cameras was 6.65%. The above values show that DeeplabV3+(ResNet-50) is this technology's most suitable semantic segmentation model. This technique can provide technical support for the scientific development of a cyanobacteria blooms management plan in the lakeshore zone of Chaohu Lake by calculating the coverage area of cyanobacteria blooms and drawing the spatial distribution map of cyanobacteria blooms in the lakeshore zone.

**Keywords:** lakeshore zone; cyanobacteria blooms; semantic segmentation; multiple threads

**Citation:** Wang, Z.; Wang, C.; Liu, Y.; Wang, J.; Qiu, Y. Real-Time Identification of Cyanobacteria Blooms in Lakeshore Zone Using Camera and Semantic Segmentation: A Case Study of Lake Chaohu (Eastern China). *Sustainability* **2023**, *15*, 1215. <https://doi.org/10.3390/su15021215>

Academic Editors: Chao Chen, Jinsong Chen, Juhua Luo and Lei Fang

Received: 11 November 2022

Revised: 25 December 2022

Accepted: 27 December 2022

Published: 9 January 2023



**Copyright:** © 2023 by the authors. Licensee MDPI, Basel, Switzerland. This article is an open access article distributed under the terms and conditions of the Creative Commons Attribution (CC BY) license (<https://creativecommons.org/licenses/by/4.0/>).

## 1. Introduction

In recent years, many nutrients have been imported into lakes with the acceleration of urbanization and the intensification of human activities in lake basins. Under the background of global warming, the water environment of inland lakes has become increasingly severe [1]. In particular, the large number of cyanobacteria blooms in the lakeshore zone not only destroys the ecological balance of lakes and reduces the ecological function of inland lakes [2], but also directly threatens the safety of drinking water by producing black and smelly water bodies [3]. Previous studies have shown that, in the

past 40 years, 21,878 lakes around the world have been plagued by cyanobacteria blooms, and the frequency of cyanobacteria blooms in the lakes of all continents (except Oceania) has increased significantly since 2010, with the most significant increase being in Asian and African countries [4]. In Chaohu lake, a typical large-scale eutrophication lake in our country, the problem of cyanobacteria blooms is outstanding and has attracted extensive attention from scholars around the world [5,6]. Relevant data show that the frequency of blue cyanobacteria blooms in Chaohu Lake has been relatively high in the past two decades. The outbreak time generally starts in February and lasts until January next year. Summer and autumn are the hot time for large-scale outbreaks of cyanobacteria blooms. The area of cyanobacteria blooms is also at a high level all year round, and the area of cyanobacteria algal blooms exceeding 100 km<sup>2</sup> also happens frequently [7,8]. Given the above situation, Chaohu Lake can become a representative example of this study lake's cyanobacteria blooms monitoring work.

In the time of the concentrated outbreak of cyanobacteria blooms in lakes, many cyanobacteria blooms often float in the surface water of the lakeshore zone, which is easy to form cyanobacteria blooms accumulation and decay, which seriously threatens the safety of drinking water. Real-time and accurate monitoring of cyanobacteria blooms in the surface water in this area can provide timely and accurate information on the coverage area of cyanobacteria blooms in the surface water of lakeshore zone for cyanobacteria administrators, help to accurately locate the coverage with the severe accumulation of cyanobacteria blooms, and timely formulate a treatment plan for cyanobacteria blooms. Currently, the commonly used cyanobacteria blooms monitoring methods include site-based cyanobacteria blooms monitoring and remote sensing-based cyanobacteria blooms identification [9,10]. While the cyanobacteria blooms monitoring based on the site can accurately obtain many water quality parameters, it is time-consuming and challenging to meet the needs of large-scale cyanobacteria blooms change monitoring [11]. With its characteristics of solid timeliness and wide monitoring range, remote sensing technology has become one of the essential tools for monitoring and predicting cyanobacteria blooms and has been widely used in monitoring and studying the Spatio-temporal dynamic changes of cyanobacteria blooms [12,13]. While remote sensing technology can realize the synchronous observation of the spatial distribution of cyanobacteria blooms, cyanobacteria blooms show high spatial and temporal heterogeneity under wind fields and hydrodynamic forces. Usually, they have apparent horizontal migration and vertical mixing at the hourly scale [14]. Limited by the frequency of satellite observation, it is difficult to capture the rapid dynamic change process of cyanobacteria blooms days [15]. In addition, due to the limitation of the spatial resolution of remote sensing images, the monitoring method of cyanobacteria blooms based on satellite remote sensing cannot effectively monitor the intensity of cyanobacteria blooms in the lakeshore zone. Therefore, how to carry out accurate monitoring, early warning, and prevention of cyanobacteria blooms in the lakeshore zone of inland lakes is an essential issue in the current lake pollution control, and a new means is urgently needed.

Currently, the construction of a lakeside video monitoring network can provide real-time video images, which can monitor the spatiotemporal dynamic changes of cyanobacteria at a higher frequency [16]. However, considering that, in addition to cyanobacteria blooms and water bodies, video images are often rich in other information interference, such as roads, buildings, and vegetation, and how to identify cyanobacteria blooms in such video images accurately has become a critical problem that needs to be solved urgently. In recent years, the field of computer vision has witnessed rapid development. Semantic segmentation methods in deep learning have achieved great success in the field of image recognition [17,18], and a large number of semantic segmentation models have emerged, such as FCN [19], U-net [20], and SegNet [21]. PSPNet [22] and Deeplab [23] models provide a feasible solution for the multi-class image classification task. Moreover, with the improvement of theory and the huge development of computational power, the recognition accuracy of the semantic segmentation model is also constantly improved due

to the optimization and update of the network structure in the deep learning model. For example, the AlexNet [24], VGG [25] and ResNet [26] networks. In particular, the ResNet network is the most representative, which deepens the training depth of the network, and alleviates the problems of gradient disappearance or explosion, network degradation, and so on. Many studies have used ResNet to improve the semantic segmentation model and have achieved relatively successful results [27–29]. Therefore, this paper chooses to use the ResNet-50 network to fuse FCN, U-net, and DeeplabV3+ models to improve the recognition accuracy of cyanobacteria blooms.

This study proposed a real-time method to identify the distribution characteristics of cyanobacteria blooms in the surface water of Chaohu lake lakeshore zone using camera and semantics segmentation methods. The technique uses the DeeplabV3+(ResNet-50) model and multithreading technology to identify cyanobacteria blooms in images in real-time, which can meet the requirement of real-time monitoring and the distribution of cyanobacteria blooms in the surface water of Chaohu lake lakeshore zone and provide technical support for the scientific formulation of cyanobacteria blooms control scheme. The main work of this paper is as follows: (1) Integrating ResNet-50 network into FCN, U-net, and DeeplabV3+ semantics segmentation method, comparing the results of cyanobacteria blooms recognition before and after the three model improvements and selecting the optimal semantics segmentation model. (2) Open the thread pool with Python and acquire 43 sets of camera video images of Ring Chao Lake by the multi-threading method, to ensure that the task of semantics segmentation can be completed within one hour to achieve the effect of real-time monitoring. (3) Calculate the coverage of cyanobacteria blooms by using the identification results of cyanobacteria blooms, quantify the accumulation of cyanobacteria blooms in the lakeshore zone, and draw the distribution map of cyanobacteria blooms in the lakeshore zone of Chaohu Lake, which provides technical support for the scientific control of cyanobacteria blooms.

## 2. Study Area and Data

### 2.1. Study Area

The purpose of this study was to monitor the accumulation and distribution of cyanobacteria blooms in the lakeshore zone of Chaohu Lake. Chaohu Lake is one of the five major freshwater lakes located in the middle and lower reaches of the Yangtze River, with an area of about 780 km<sup>2</sup> and a total length of 55 km, as shown in Figure 1. According to relevant studies, Cyanophyta is dominant in the composition of phytoplankton in Chaohu Lake, and the dominant species are mainly *Microcystis* and *Anabaena Flos-Aquae*. From March to April, *Anabaena Flos-Aquae* is prevalent in the formation of water blooms in Chaohu Lake; from May to September, with the increase in temperature, *Microcystis* predominates to form water blooms; after October, the daily average temperature drops, and the water blooms are dominated by *Anabaena Flos-Aquae* [30,31]. In the past 20 years, cyanobacteria blooms have occurred frequently in Chaohu Lake [32]. Due to the influence of wind and hydrodynamic factors, the lakeshore zone of Chaohu Lake has become a critical area of cyanobacteria blooms accumulation, which not only causes harm, such as black and smelly water and water eutrophication, but also seriously threatens the safety of drinking water. Therefore, through 43 sets of cameras installed in the lakeshore zone of Chaohu Lake and the semantic segmentation method of deep learning, this study can accurately identify the distribution characteristics of cyanobacteria blooms in the lakeshore zone of Chaohu Lake in real time, accurately express the accumulation degree of cyanobacteria blooms, and provide technical support for the scientific development of cyanobacteria blooms management plan.

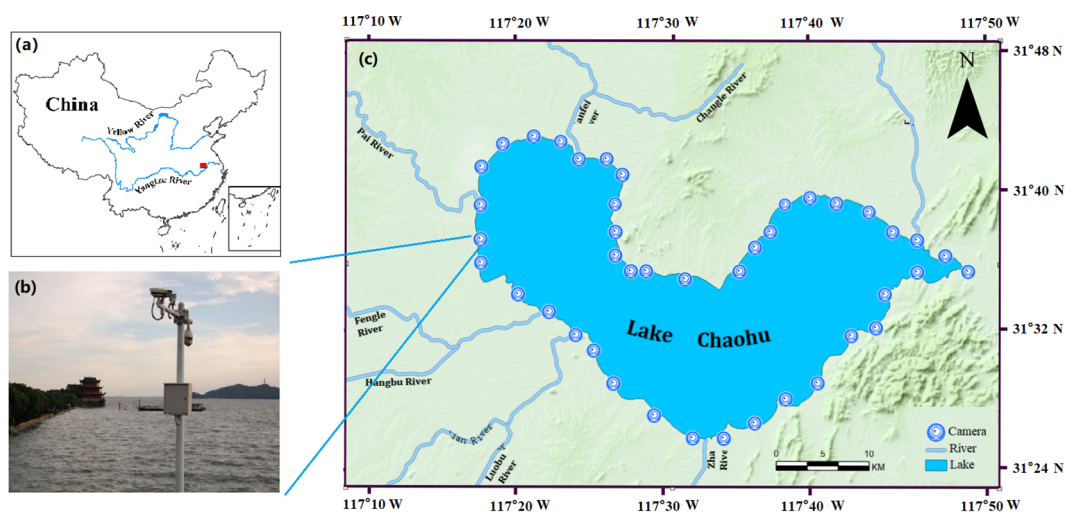


**Figure 1.** Current situation of the study area: (a) The specific location of Chaohu Lake is in China; (b) the cameras set up are in Chaohu Lake; and (c) the specific locations of 43 cameras are in Chaohu Lake.

## 2.2. Data

The data used in this study came from the video images of 43 sets of cameras around Chaohu Lake. Most locations where the cameras are set up are the mouth of the Chaohu Lake's rivers, water intake areas, and areas where cyanobacteria blooms often accumulate. The 43 sets of cameras were set up to monitor the distribution of cyanobacteria blooms along the shore of Chaohu Lake, as well as to monitor illegal fish fishing and maintain social security. To maximize the function of cameras and save costs, the number of cameras is 43 after field investigation. Therefore, the camera will adjust the monitoring angle under artificial control. The change in the monitoring angle will make the video image unable to capture the water surface information. To meet the requirements of monitoring the cyanobacteria blooms in the lakeshore zone, each camera will adjust the shooting angle according to the preset attitude parameters in the first 10 min of every hour to obtain the lake surface image of the lakeshore zone to the maximum extent. Each camera also has its own webcam video streaming address, which can be viewed by entering the address on the browser's web page. By using the selenium module of Python to take screenshots of the video streaming address images of each camera every hour from 8:00 to 18:00 and save them, the resolution of the video image data obtained is  $1920 \times 1080$ , the collection period is from September 2021 to October 2022. The collection period is one year, and a total of 188,943 images were obtained. The pictures of the sample data set are from the camera images of each month within the year so that the semantic segmentation task can be adapted to the cyanobacteria bloom identification scene in each month.

## 3. Method

### 3.1. Cyanobacteria Blooms Identification Process

The specific process of cyanobacteria blooms recognition is shown in Figure 2, which is the same as other image segmentation tasks. First, use labelme tools to make sample datasets. To improve the accuracy of cyanobacteria blooms identification, encoders of FCN, U-net, and DeeplabV3+ models were modified and trained using the ResNet-50 network, and the optimal models were evaluated according to the segmentation results. Cyanobacteria blooms identification should be completed within one hour to ensure real-time monitoring of the hourly dynamic changes of the cyanobacteria blooms along the lake shore. A thread pool was created through python's threading module, and threads were distributed through the thread pool to reduce the task execution time. The specific tasks to be executed by the thread are as follows: Obtain 43 sets of video stream pictures from

cameras every hour and input the obtained images into the trained semantic segmentation model for cyanobacteria blooms identification. The coverage of cyanobacteria blooms was calculated to quantify the accumulation degree of cyanobacteria blooms in the lakeshore zone, and the spatial distribution map of cyanobacteria blooms in the lakeshore zone of Chaohu Lake was drawn.

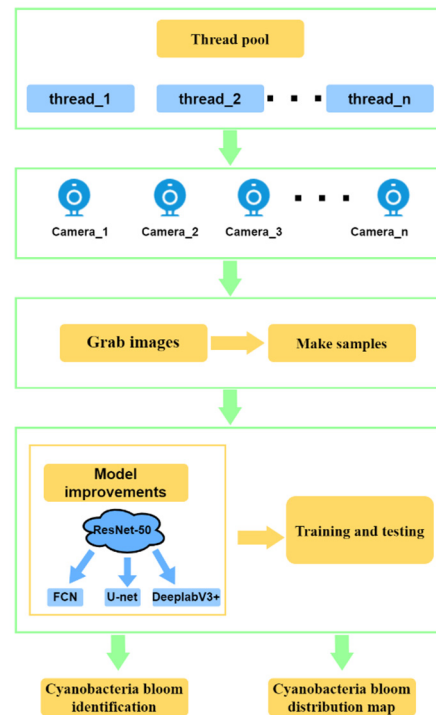


**Figure 2.** Flowchart of real-time identification of cyanobacteria blooms.

### 3.2. Multi-Thread Mechanism Construction

When acquiring video images, we will encounter a challenging problem: Due to the slow network speed, it takes more time to load the camera video stream, which will put pressure on the time required for subsequent models to identify cyanobacteria blooms, and it may be impossible to fully obtain the cyanobacteria blooms distribution information in the Chaohu Lake lakeshore zone within one hour. To solve this problem, the multi-threading technology can set multiple thread plans to enable tasks to process processes in an asynchronous manner [33,34]. The management of the number of threads can rely on the thread pool. The role of the thread pool can uniformly manage threads. Under the constraint of the maximum number of threads, the number of threads can be selected independently, reducing resource consumption, improving response speed, and reserving space for adding subsequent functions [35]. The specific process of thread creation is shown in Figure 3. First, create a thread pool and set the maximum number of threads. The thread queue in the thread pool is divided into two parts: the core thread queue and the waiting thread queue. When the task is initiated, select threads from the core threads to execute the task. When the number of tasks exceeds the number of core threads, use the threads in the waiting queue to execute the task. If the core thread queue and the waiting thread queue have no idle threads to use, the execution rejection strategy will be implemented. The execution rejection strategy in this study is to find the free threads to execute the task after the task has been waiting for execution for 5 min.



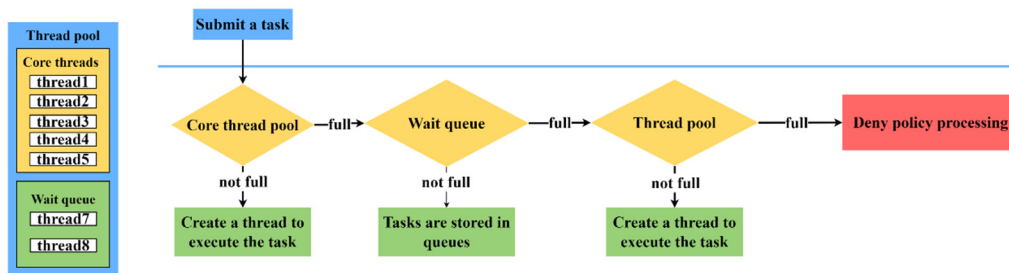


**Figure 3.** Process pool task execution process.

The increase in the number of threads can reduce the task's execution time, but too many threads will bring more pressure to the server's CPU and threaten the normal operation of other tasks on the server, thus causing the collapse of the task process. Therefore, after multiple tests on 43 cameras on a 2vCPU-4GIB server with 8M network bandwidth, the number of threads is set, as shown in Table 1. In the process of increasing threads from 1 to 7, the processing time of the task decreases step by step. The task processing time can be basically controlled within 60 min for the number of threads more than 4 times. However, when the number of threads reaches 6, the CPU load is up to 92.5%, which will cause interference with other processes in the server. However, in the case of unexpected camera shutdown and network crash, not all 43 sets of camera images will participate in the task. Even 2 to 3 threads can meet this case's task processing time requirements. Therefore, use the python threadpool module to create a thread pool. The maximum number of threads is 7, the number of threads in the core thread queue is 5, and the number of threads waiting for the thread queue is 2.

**Table 1.** Thread number selection table.

| Number of Threads | Average Time (min) | CPU Load (%) |
|-------------------|--------------------|--------------|
| 0                 | 67                 | 41.8         |
| 1                 | 59                 | 42.9         |
| 2                 | 58                 | 53.6         |
| 3                 | 56                 | 75.2         |
| 4                 | 51                 | 78.6         |
| 5                 | 46                 | 89.1         |
| 6                 | 45                 | 92.5         |
| 7                 | 43                 | 98.7         |

### 3.3. Sample Set Production

The video images obtained after adjusting the camera attitude still cannot guarantee that there are no other ground objects except cyanobacteria blooms and water bodies in all the pictures. Given this situation, to better evaluate the accuracy of cyanobacteria blooms recognition in the recognition results, the recognition task of cyanobacteria blooms is defined as multiple classification tasks to intuitively compare whether the cyanobacteria blooms and the boundary segmentation between water bodies and other ground objects are accurate. As shown in Figure 4, the labelme tool was used for sample labeling. Sample labels were divided into six categories, namely cyanobacteria blooms (green), water (blue), road (purple), vegetation (red), sand (yellow), and other categories (black). The scope of sample selection includes video image files of all 43 cameras and image files containing all ground object types. In addition, image files with shadows and water ripples are added to evaluate the semantic segmentation model from more perspectives. The image resolution was  $1920 \times 1080$  and 1736 samples were made. Through translation, scaling, inversion, and fuzzification of image augmentation technology, the samples were increased to 3126. Of that, 80% is used to train the model, and 20% is used to validate the model.

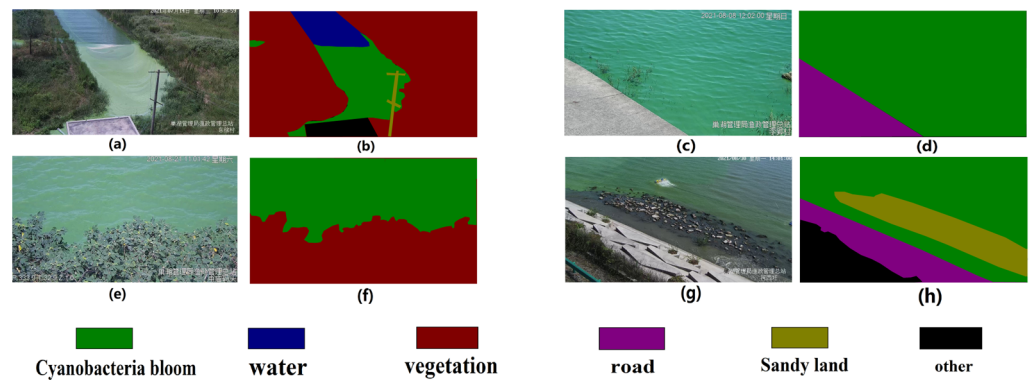


**Figure 4.** Sample original picture and label picture: (a,c,e,g) are camera original pictures; (b,d,f,h) are label pictures.

### 3.4. Model Improvement and Training

In recent decades, semantic segmentation methods based on convolutional neural networks (CNN) have achieved good results in image segmentation, including FCN, SegNet, U-net, PSPNet, DeeplabV3+, and other methods. This paper uses three classical semantic segmentation methods (FCN, U-net, and DeeplabV3+) to evaluate the performance of cyanobacteria blooms recognition [36]. In addition, the ResNet-50 network was chosen to integrate the three semantic segmentation methods that were investigated in this study so that the number of parameters used in the process of semantic segmentation could be decreased, the network depth could be increased, the convergence of training could be completed more quickly, and the classification accuracy could be increased. ResNet-50 is based on the traditional linear convolution network structure for the purpose of increasing a fast connection. Its design is illustrated in Figure 5, and it works as follows: The input image first, after steps 2 and  $7 \times 7$  convolution kernels of convolution operation, the size of the input image is reduced twice. Finally, the image size is reduced once more through a top pooling layer. Among the four bottleneck residual blocks, each residual module contains two convolution layers, an activation function layer, and two batch normalization layers. The size of the convolution kernel in the convolution layer is  $3 \times 3$ , and the underlying parameters can be relocated to the next layer through a shortcut connection, and the jump connection can prevent the gradient loss during backpropagation [26].

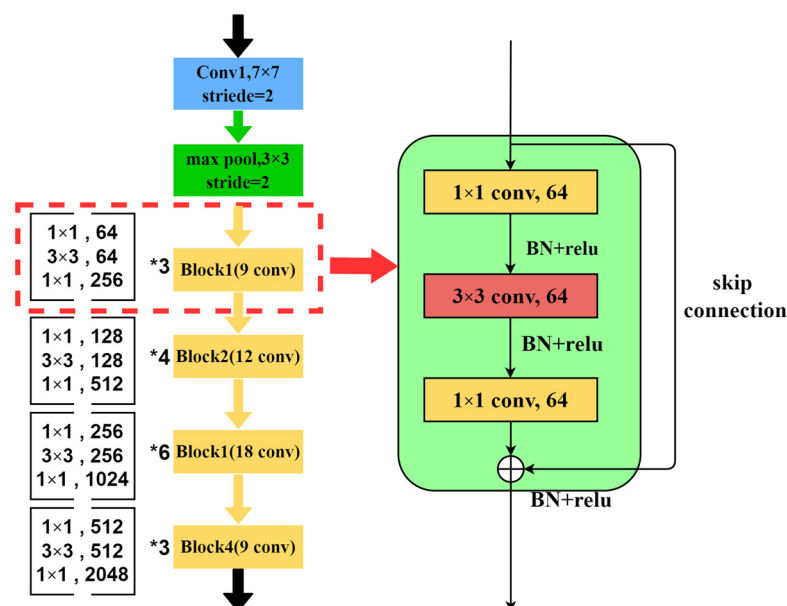


**Figure 5.** Network structure of ResNet-50.

The network structure of the three semantic segmentation methods is composed of an encoder to extract the image features and a decoder to locate the image features. In this study, ResNet-50 is employed as the primary network structure for the encoder of the three semantic segments. In the decoder portion of FCN, the fully connected layer and pooling layer of the original convolutional network are eliminated and replaced with  $1 \times 1$  convolution and transposed convolution. Through network layers, such as the deconvolution layer [37], the target's specifics and corresponding spatial dimensions are gradually recovered. The decoder part of the U-net consists of an up-sampled convolution layer, feature concatenation, and two  $3 \times 3$  convolution layers with a step size of 1. The up-sampling method uses deconvolution to double the feature map size, concatenation, and two convolution layers to fuse the features prior to and after up-sampling [38]. The decoder part of DeeplabV3+ extracts the low-level feature map from the second convolution block of ResNet-50. The output multi-scale high-level feature map is combined with the low-level feature map using a series of convolution operations and the up-sampling method of bilinear interpolation. Following a bilinear interpolation, the image size is restored to conclude the image segmentation task [39,40].

2501 photos were used for training the three models, and the remaining 635 photos were used as the verification set of the model. The three models use the same training set and verification set. The model is trained and verified in NVIDIA GeForce GTX 1660Ti mobile graphics card, and the processor is an Intel i7-9750H CPU @ 2.60 GHz  $\times$  8–12 processor. The training time of the three models takes 595 min on average. The three semantic segmentation methods all perform 100 epochs. Each epochs contains 80 steps. The loss function uses the cross entropy loss function. With the Adam optimizer, the learning rate is  $1 \times 10^{-4}$  [41]. Since the ResNet-50 network is used, use pre-trained parameters to initialize the default weight value. The performance of the three semantic segmentation methods for cyanobacteria blooms recognition is evaluated by comparing with the real image of the camera image. The segmentation results were compared with the natural mask of the sample, and the following indexes were calculated. The IOU is shown in Formula (1). The Mean Intersection Over Union (mIOU) is shown in Equation (2). The MPA is shown in Equation (3). The OA is shown in Equation (4).

$$IOU = \frac{TP}{(TP + FP + FN)} \quad (1)$$

$$mIOU = \frac{\sum_i ii}{N(\sum_i \sum_j x_{ij} + \sum_j x_{ji} - x_{ii})} \quad (2)$$

$$MPA = \frac{i}{N+1} \sum_{i=0}^n \frac{X_{ii}}{\sum_{j=0}^n X_{ij}} \quad (3)$$

$$OA = \frac{\sum_{i=1}^N x_{ii}}{\sum_{i=1}^n \sum_{j=1}^n x_{ij}} \quad (4)$$

where  $N$  represents the number of classes,  $x_{ij}$  represents the number of pixels of prediction class  $i$  as class  $j$ , and  $x_{ii}$  represents the number of correctly predicted pixels.  $TP$  is the number of positive classes predicted by actual positive classes;  $FN$  is the number of negative classes predicted by actual positive classes; and  $FP$  is the number of positive classes predicted by actual negative classes.

### 3.5. Calculation of Cyanobacteria Blooms Coverage

The identification results of cyanobacteria blooms are aimed at the distribution of cyanobacteria blooms on the surface of the lakeshore zone waters. To quantitatively express the cyanobacteria biomass in the region's surface waters, the coverage rate of cyanobacteria blooms is proposed. For the camera pictures adjusted according to the preset pose parameters, the cyanobacteria blooms coverage rate, and the cyanobacteria biomass of



the surface water body show a positive proportion relationship. The cyanobacteria blooms coverage rate under different values can provide an additional reference for managing cyanobacteria blooms in the lakeshore zone. The calculation method of cyanobacteria blooms coverage can be divided into two steps. In the first place, count the number of pixels in the cyanobacteria blooms area and the number of pixels in the non-cyanobacteria blooms water body in accordance with the RGB color value and subsequently divide the number of pixels in the cyanobacteria blooms area and the number of pixels into the two areas, and present them in percentage. The formula is shown in (5):

$$P = \frac{B_{num}}{W_{num} + B_{num}} \times 100\% \quad (5)$$

$P$  represents the coverage of cyanobacteria blooms. The greater the percentage value, the more severe the accumulation; the smaller the value is, the less severe the accumulation is ( $P \in [0.00\%, 100.00\%]$ ).  $B_{num}$  represents the number of pixels in the cyanobacteria blooms area, and  $W_{num}$  denotes the number of pixels in the water area.

By comparing the calculated coverage of cyanobacteria blooms with the actual mask value of cyanobacteria blooms, the identification performance of the Root Mean Square Error (RMSE) evaluation method was calculated, and the formula was shown in (6):

$$RMSE = \sqrt{\frac{\sum_i (P_m - P_a)^2}{N}} \quad (6)$$

$P_m$  is the cyanobacteria blooms coverage value calculated using the results identified by the semantic segmentation model,  $P_a$  is the actual cyanobacteria blooms coverage value, and  $N$  is the number of photos used.

## 4. Result

### 4.1. Identification of Cyanobacteria Blooms

The loss and accuracy curves are plotted during model training, as indicated in Figure 6. The loss is the total error of each image sample in the training and testing stages, and it represents the performance of the model after each epoch. The three models all demonstrate good convergence speed. After 60 epochs, the jitter potential tends to be flat, and the jitter range is between 0.08 and 0.25. The training loss of DeeplabV3+(ResNet-50) closely resembles the jitter value of the test loss. The accuracy curves of the three models also indicate a good convergence effect. DeeplabV3+(ResNet-50) has the highest accuracy value in training and testing, between 0.82 and 0.86. FCN(ResNet-50) had the lowest training and testing accuracy, ranging from 0.78 to 0.81. U-net's (ResNet-50) training and testing accuracy values are in between.

The image segmentation performance of the six models was evaluated by comparing the six models' mIOU, MPA, IOU(cyanobacteria blooms, water) and OA indexes. The results are shown in Table 2. After the integration, the index values of the three models have been significantly enhanced, and the range of the enhancement is between one and three percent. In comparison to the other two integrated models, the performance of the FCN(ResNet-50) model is poor, and the values of OA, MPA, mIOU, and IOU(cyanobacteria blooms and water) all occupy the lowest level. The MPA value of the U-net(ResNet-50) model is similar to that of the DeeplabV3+(ResNet-50) model, but the values of OA, mIOU and IOU (cyanobacteria blooms and water) of the U-net model are slightly lower than those of the DeeplabV3+(ResNet-50) model. DeeplabV3+(ResNet-50) has a superior performance based on the analysis of the four preceding metrics, but the gap between DeeplabV3+(ResNet-50) and U-net(ResNet-50) is relatively small.

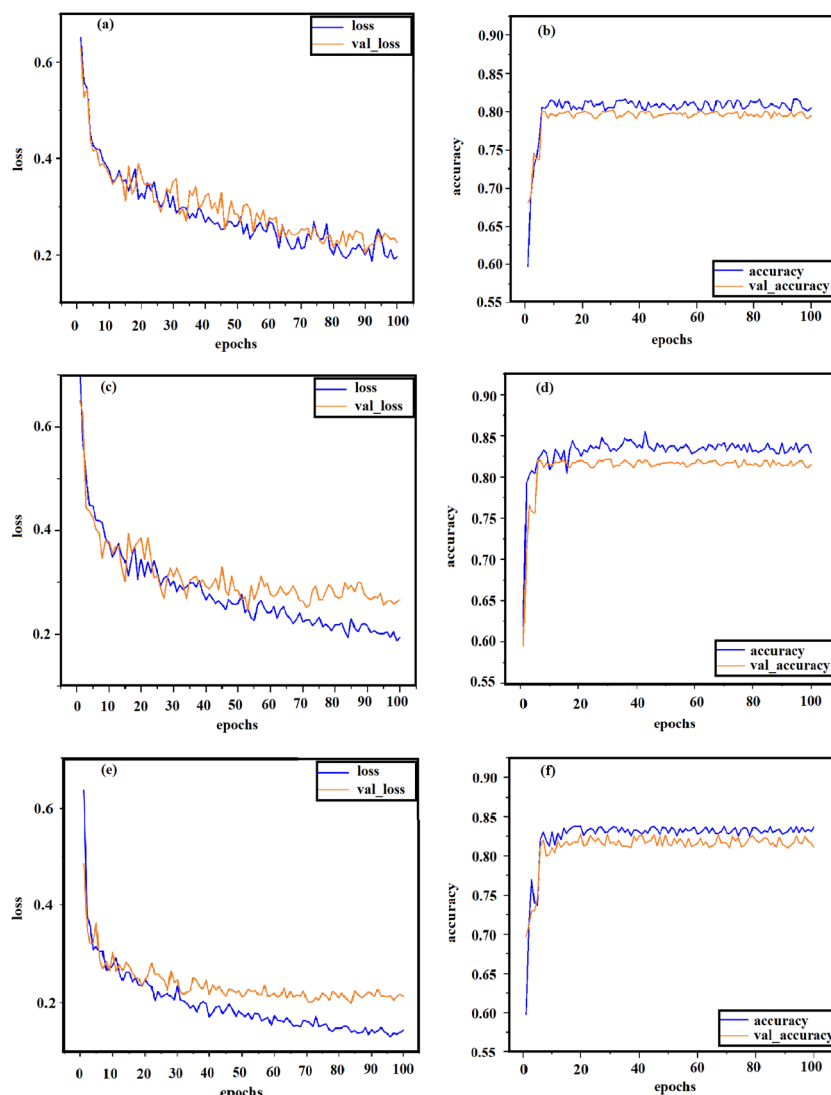


**Figure 6.** Loss Chart and Accuracy Chart: (a,c,e) are FCN(ResNet-50), U-net(ResNet-50), and DeeplabV3+(ResNet-50) loss charts respectively; (b,d,f) are FCN(ResNet-50), U-net(ResNet-50), and DeeplabV3+(ResNet-50) accuracy charts correspondingly.

**Table 2.** OA, MPA, mIOU, and IOU of six model evaluation forms.

| Method                | OA (%) | MPA (%) | mIOU (%) | Cyanobacteria Blooms-IOU (%) | Water-IOU (%) |
|-----------------------|--------|---------|----------|------------------------------|---------------|
| FCN                   | 76.96  | 77.54   | 67.73    | 66.38                        | 68.43         |
| U-net                 | 78.24  | 78.63   | 68.43    | 68.29                        | 70.25         |
| DeeplabV3+            | 80.29  | 79.84   | 69.82    | 69.46                        | 71.24         |
| FCN(ResNet-50)        | 79.42  | 78.41   | 67.36    | 68.73                        | 70.26         |
| U-net(ResNet-50)      | 81.21  | 80.68   | 71.23    | 70.03                        | 72.43         |
| DeeplabV3+(ResNet-50) | 83.27  | 81.78   | 72.42    | 71.65                        | 74.38         |

Intending to compare the performance of cyanobacteria blooms recognition before and after the model integration in a more intuitive manner, 12 images containing all image segmentation categories are chosen, as demonstrated in Figure 7. The six models are capable of identifying cyanobacteria blooms based on the segmentation results of eleven images. Additionally, all six models performed equally well for an image full of cyanobacteria blooms (yellow box in Figure 7). The identification performance of the

three models containing cyanobacteria blooms in long-shot photographs was poor before integration. In comparison to the DeeplabV3+(ResNet-50) and U-net(ResNet-50), the cyanobacteria blooms identified by the FCN(ResNet-50) failed to identify cyanobacteria blooms. The cyanobacteria blooms area estimated by the U-net(ResNet-50) is significantly smaller than the actual blooms area (as shown in the red circle in Figure 7). For the overlapping area of cyanobacteria blooms and surface ripple, the accuracy of cyanobacteria blooms identification by the FCN(ResNet-50) and DeeplabV3+(ResNet-50) is significantly improved, particularly the segmentation of the junction of cyanobacteria blooms and other ground features is more accurate. Nonetheless, the consequences of cyanobacteria blooms identification before and after U-net integration were similar, and the accuracy of recognition did not improve. DeeplabV3+ is sensitive to overlapping areas of cyanobacteria blooms and surface ripples. It can accurately identify boundary information (as depicted in the pink circle in Figure 7), which may be why DeeplabV3+ fuses low-level features with high-level features to improve the accuracy of boundary segmentation. The image of cyanobacteria blooms is not visible in the cyanobacteria blooms area with bright vista light, and the DeeplabV3+(ResNet-50) has a particular advantage in recognizing cyanobacteria blooms in this area, followed by the U-net(ResNet-50). At the same time, FCN ignores the glory of cyanobacteria blooms in this area (as demonstrated in the green circle in Figure 7). The spatial state of cyanobacteria blooms distribution can be identified accurately by all six models (as shown in the golden circle in Figure 7). For the shaded areas that often appear at the junction of cyanobacteria blooms and coastal roads, grassland, and sandy land, the six models have relatively accurate identification effects (as shown in the purple circle in Figure 7). As for the shaded regions of other regions, the accuracy of the six models was greatly disturbed (as indicated in the red circle in Figure 7). For images with weak light intensity, the cyanobacteria blooms results identified by the improved model are more accurate, particularly the cyanobacteria blooms area identified by the DeeplabV3+(ResNet-50), which is more similar to the real mask image (as indicated in the blue circle in Figure 7). At the interface between cyanobacteria blooms and water bodies, the spatial distribution shape of cyanobacteria blooms is typically irregular and ribbon-like. For the cyanobacteria blooms identification task in this area, the FCN, and DeeplabV3+ models before integration perform relatively poorly, with a weak response to the recognition of small patches. Nonetheless, the FCN(ResNet-50) model rectified the initial erroneous cyanobacteria blooms location. The identification results of cyanobacteria blooms in the DeeplabV3+(ResNet-50) model were quite similar to the real mask image, while the consequences before and after the integration of the U-net model showed no significant changes (as indicated in the green circle in Figure 7). For the image's text area, the accuracy of the six models is comparable. Moreover, for the image of mixed turbidized water and cyanobacteria blooms, the identification result of the DeeplabV3+(ResNet-50) has the closest resemblance to the actual mask (see the brown circle in Figure 7). The areas within cyanobacteria blooms identified by the six models are frequently accompanied by holes, due in part to the disruption of organisms and camera-style rainfall. In combination with the calculated performance indicators and the comparison results of cyanobacteria blooms identification, the DeeplabV3+(ResNet-50) network model was selected as this study's final semantic segmentation model.

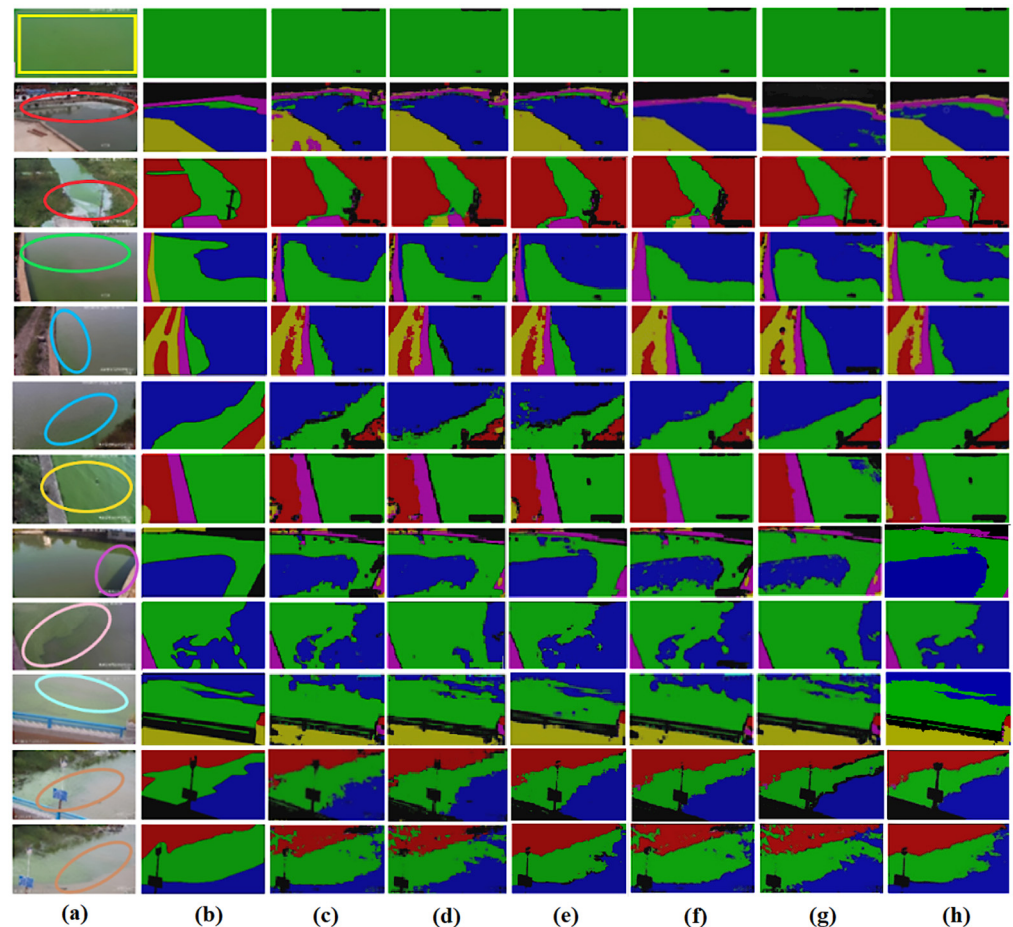


**Figure 7.** Comparison of cyanobacteria blooms identification results: (a) is the original image; (b) is the real mask image; (c–e) are the results of cyanobacteria blooms identified by FCN, U-net, and DeeplabV3+ before improvement; and (f–h) are the results of cyanobacteria blooms identified by FCN(ResNet-50), U-net(ResNet-50), and DeeplabV3+(ResNet-50).

#### 4.2. Calculation of Cyanobacteria Blooms Coverage

The images of 43 cameras with common angles around Chaohu Lake were input to the DeeplabV3+(ResNet-50) model for cyanobacteria blooms identification, and subsequently, the recognition effect of DeeplabV3+(ResNet-50) in all common camera scenarios was evaluated. It should be noted that, due to the location of certain coastal areas, even when Chaohu Lake has a high concentration of cyanobacteria blooms, cyanobacteria blooms rarely accumulate in coastal areas. Consequently, most of the time, some camera images are only in the water area. As indicated in Figure 8, on the basis of the overall analysis of the cyanobacteria blooms recognition results of 43 cameras, the DeeplabV3+(ResNet-50) can accurately identify the spatial distribution of cyanobacteria blooms and accurately depict the water body, the boundary between algal blooms and the shore in images with a few types of ground objects and close up pictures. Moreover, DeeplabV3+(ResNet-50) can identify the spatial information of cyanobacteria blooms from distant images with precision. DeeplabV3+(ResNet-50) also provides satisfactory recognition results at the junction of multiple feature types for images with numerous features. Shadows and wavy reflective water surfaces have a small impact on DeeplabV3+(ResNet-50)'s recognition of cyanobacteria blooms. For images with other surface features on the water surface, DeeplabV3+ can also accurately exclude these features from the identification of cyanobacteria blooms and water body. Nonetheless, DeeplabV3+(ResNet-50) did not accurately separate the images of turbid water bodies and cyanobacteria blooms. Consequently, the problem may be



that the pixel context information in this area is complex, and the image resolution is low. In accordance with the analysis of the total combined outcomes of the identification of cyanobacteria blooms by 43 cameras, DeeplabV3+(ResNet-50) is capable of accurately identifying cyanobacteria blooms in the lakeshore zone surrounding Chaohu Lake.

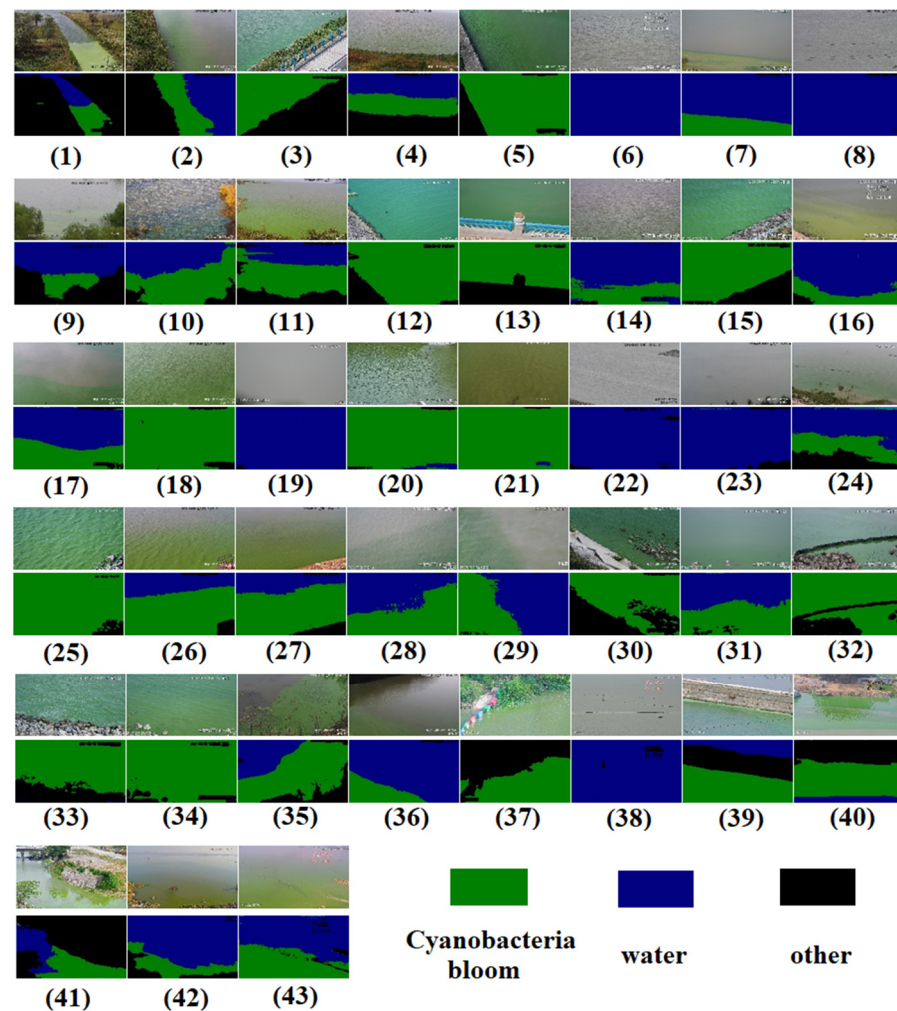


**Figure 8.** Common scene pictures of 43 cameras in Chaohu Lake and identification results of cyanobacteria blooms.

Collect the predicted value of the cyanobacteria blooms coverage of 43 cameras and the cyanobacteria blooms coverage of the real mask of the image, and make a 1:1 scatter plot, as indicated in Figure 9. On the whole, the  $R^2$  is 0.98 and the RMSE value is 6.65%. Twenty-six of the 43 predicted cyanobacteria blooms coverage values are lower than the actual cyanobacteria blooms mask coverage, but the difference is between 2% and 9%, and the recognition error falls within the acceptable range. There are four cyanobacteria bloom prediction values that are the same as the actual mask values. Additionally, these four images only contain water body areas, with no surface features interfering. This demonstrates that DeeplabV3+(ResNet-50) accurately identifies water bodies in these images, which is similar to the actual situation. In the six pictures with dense coverage of cyanobacteria blooms, four of the predicted values of cyanobacteria blooms are lower than the real ones, while the remaining two are the opposite. The range of the total error is between two and four percent. This error displays that DeeplabV3+(ResNet-50) is also applicable to the pictures with a high coverage of cyanobacteria blooms.



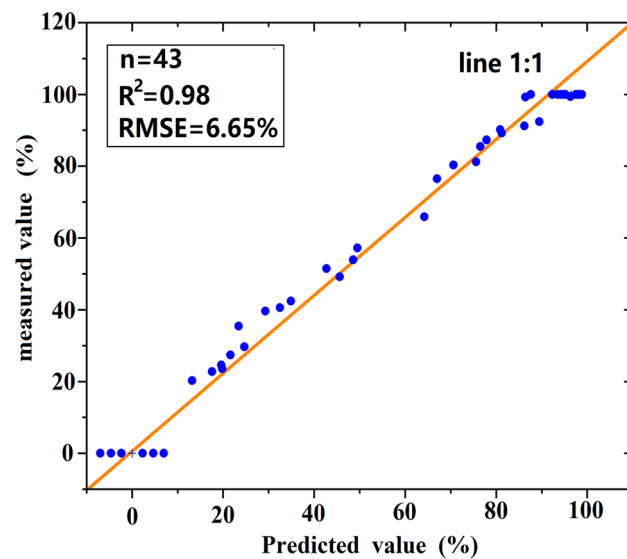


**Figure 9.** Verification of cyanobacteria blooms identification results from 43 cameras in Chaohu Lake.

#### 4.3. Chaohu Case Study

The experiment was conducted from 8:00 a.m. to 6:00 p.m. on 1 September 2022, and 8:00 a.m. to 6:00 p.m. on 30 September 2022, to assess the viability of the cyanobacteria blooms recognition task. The period was one month, and the reason for the selection was an outbreak of cyanobacteria blooms in Chaohu Lake this month. Calculate the average task execution time at eleven-time points during the current month. As demonstrated in Figure 10, the blue color is the average time after statistics, and the number of photos used to identify tasks is represented by the yellow color. Due to the fact that the camera maintenance downtime, the average number of photos extracted per hour is between 34 and 36, the average time for task execution per hour is within 45 min, the average execution time for each photo is 1.3 min, and the number of threads automatically started by the thread pool is four–six. On the condition that 43 lakeshore zone pictures of the whole lake are recognized every hour, the total time can be managed within one hour, which fulfills the overall requirements of the study.

To further check the identification of cyanobacteria blooms on a specific day during the experimental period, the identification results of cyanobacteria blooms on 17 September 2022 were selected, and a hotspot map was drawn in accordance with the coverage of cyanobacteria blooms, as indicated in Figure 11. On this day, 43 sets of cameras along the Chaohu Lakeshore were all involved in the cyanobacteria blooms recognition task. A total of 10 cameras showed null values in the hotspot map of cyanobacteria blooms coverage, especially for cameras No. 2, No. 4, and No. 5. After investigation, it was found that the three cameras were offline at the time when the null value appeared. A total of 13 sites detected cyanobacterial blooms coverage of more than 50%, indicating that the area of these camera sites had a severe cyanobacterial blooms accumulation on that day. From the time scale analysis, there are 55 camera pictures with a coverage rate of cyanobacteria blooms exceeding 30%, among which 44 are obtained from 10:00 to 16:00, indicating that this period is the hot time of cyanobacteria blooms accumulation. In contrast, the coverage rate of cyanobacteria blooms in other periods is less than 20%. The reason for the sudden decrease of cyanobacteria blooms coverage in two adjacent periods was found to be caused by the artificial fishing of cyanobacteria. In the subsequent step, the spatial distribution of cyanobacteria blooms accumulation will be combined to further validate the accuracy of cyanobacteria blooms identification.

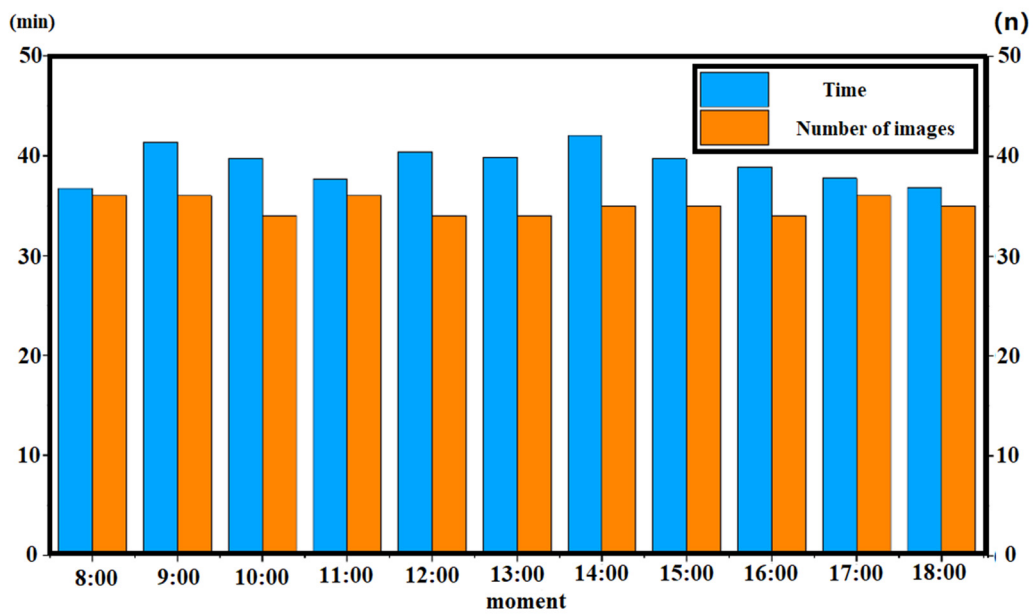


**Figure 10.** Number of images and average time of task execution per hour: The blue bar graph shows the monthly average time of task execution (left y-axis); orange is the average number of images performed per month (right y-axis).

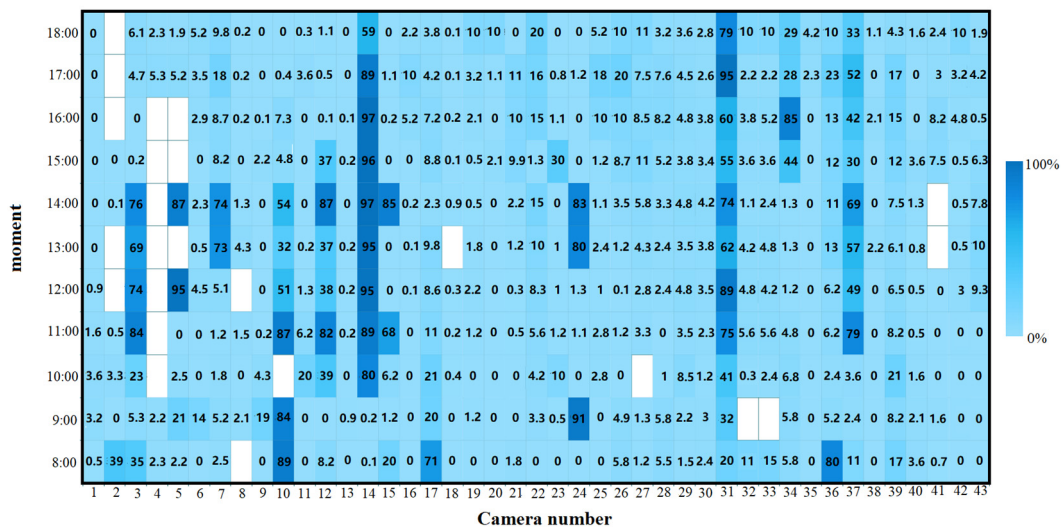


**Figure 11.** Hot spots of blue algae bloom coverage.

The spatial distribution map of cyanobacteria blooms in the lakeshore zone of Chaohu Lake was drawn by applying the proportion values of cyanobacteria blooms accumulated from each camera site. As displayed in Figure 12, the images prove 8:00, 11:00, 14:00, and 18:00 on 17 September 2022: The distribution of cyanobacteria blooms in the Chaohu Lake lakeshore zone. The analysis of image results indicated that the spatial distribution of cyanobacteria blooms in the lakeshore zone of Chaohu Lake changed significantly within a day, and there were 13 hotspots of blooms throughout the day, most of which were situated near urban villages and river estuaries. 8:00 is the initial time for identifying cyanobacteria blooms, and three areas demonstrate a high accumulation of cyanobacteria blooms. All of the photographs taken by the camera are close-up images, the shooting area of the overall water area is small, and the identification consequence of the cyanobacteria blooms is accurate. At 11:00, there were seven hot spots of cyanobacteria blooms accumulation. In accordance with the pictures, the brightness of the images becomes intense. The seven

pictures contain other surface feature types except for water bodies and cyanobacteria blooms, and reflective ripples appear on the water surface, and yet the recognition results of cyanobacteria blooms are more accurate. However, the three hot spots appeared at 8:00 have disappeared, which is considered to be caused by the artificial salvage of cyanobacteria blooms. The spatial distribution map of cyanobacteria blooms at 14:00 indicates that the accumulation of cyanobacteria blooms in the lakeshore zone of Chaohu Lake is severe at this moment in time, and there are heavy accumulations of cyanobacteria blooms in the east, west, and central and three regions of the lake area. In combination with photo comparison information, the identification results of cyanobacteria blooms are relatively accurate, which could be caused by the increasing temperature and wind speed, leading to this situation at this time. The identification of cyanobacteria blooms concluded at 18:00. Consequently, the results showed that four areas were identified as hot spots. Notwithstanding, due to the low light, the two hot spots in the upper half of the lake area were not distinguishable by the naked eye. The percentage of cyanobacteria blooms in the other two identified cyanobacteria blooms is also low. Nonetheless, these areas are still defined as hot spots because the accumulation of cyanobacteria blooms in other areas is lower than that in these four areas, which proves that at 18:00, with the temperature decreasing, the sun weakens. There is no severe accumulation of cyanobacteria blooms in the Chaohu Lake lakeshore zone as a result of artificial salvage.

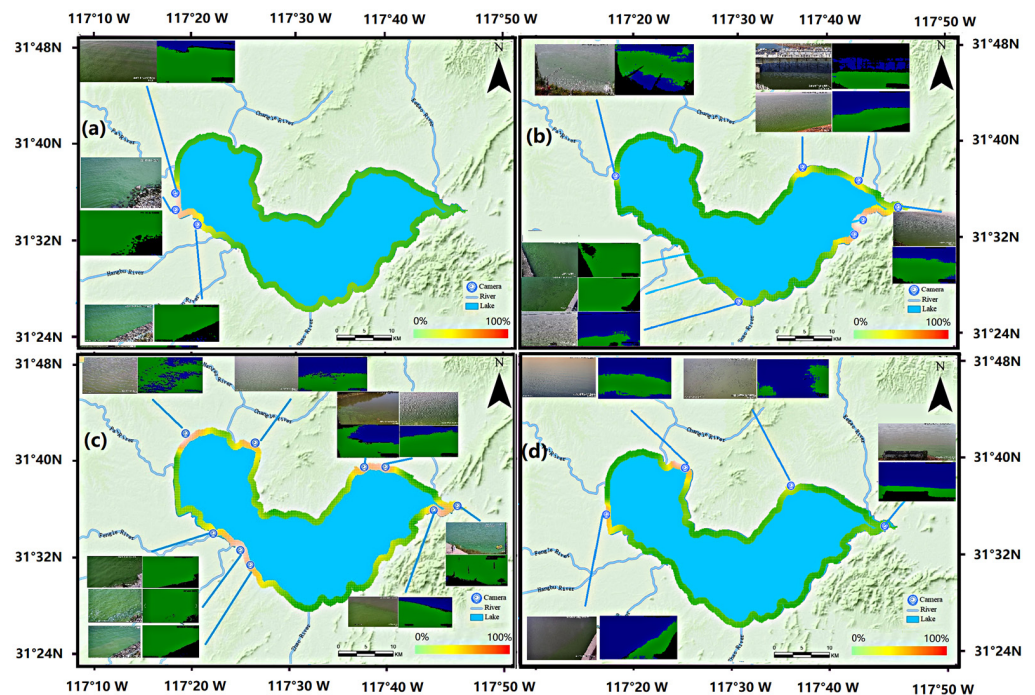


**Figure 12.** Statistics of the number of images and the average time required per hour to complete a task: (a) is the cyanobacteria blooms distribution at 8:00, (b) is the cyanobacteria blooms distribution at 11:00, (c) is the cyanobacteria blooms distribution at 14:00, and (d) is the cyanobacteria blooms distribution at 18:00.

## 5. Discussion

Compared to the monitoring method based on site, the monitoring method provided in this study can save cost and meet the needs of large-scale monitoring. Monitoring based on satellite data can achieve the effect of low cost. Currently, satellite sensor data commonly used for cyanobacteria bloom monitoring include Modis, Landsat, and MSI [42–44]. However, the highest spatial resolution of these widely used satellite data is 10 m (MSI, acquisition cycle is ten days), and the shortest acquisition cycle is two scenes a day (Modis, resolution is 250 m), which is challenging to meet the needs of real-time and accurate monitoring.

The monitoring method in this study can avoid the influence of sizeable spatial resolution of remote sensing data (most remote sensing image pixels in the lakeside zone are mixed pixels) and long acquisition period to monitor the distribution of cyanobacteria accurately blooms in the lakeside zone on an hour scale.

However, some aspects of this study also need to be further studied and solved. For example, in rainy weather, raindrops in camera images will interfere with camera imaging results. Due to the camera angle, only a tiny amount of water is included in the picture when measuring the coverage of cyanobacteria blooms due to the camera angle, but there are a large number of cyanobacteria blooms in a small amount of water. In this case, when calculating the coverage of cyanobacteria blooms, a large proportion of cyanobacteria blooms will be recorded, but it does not mean the accumulation degree of cyanobacteria blooms in this area is serious.

In the follow-up study, we will focus on the above issues and conduct in-depth research. For example, consider whether to introduce rainproof camera hardware [37], add more sample datasets with small shooting angles and rich shadows, and introduce other semantic segmentation mechanisms to improve network models' accuracy of cyanobacteria bloom recognition. For the problems in measuring the coverage of cyanobacteria blooms, consider adding a spatial mechanism to count the specific area of cyanobacteria blooms while counting the range of cyanobacteria blooms to evaluate the accumulation degree and distribution status of cyanobacteria blooms in lakes from more perspectives.

## 6. Conclusions

Effectively monitoring cyanobacteria blooms in the lakeshore zone of lakes can support the scientific formulation of the cyanobacteria blooms control scheme. Considering the high spatial resolution and weak timeliness of cyanobacteria blooms monitoring method based on satellite data. This study aims to provide a real-time and accurate identification technology for cyanobacteria blooms on the lake shoreline. This technology defines the cyanobacteria bloom identification task as an image segmentation problem. It uses the multi-thread technology and real-time images provided by the camera around the lake and uses the DeeplabV3+(Resnet-50) model for real-time recognition of cyanobacteria bloom in the camera images. The novelty of this work lies in the accurate monitoring of the distribution of cyanobacteria blooms on the 11 h scale every day, and the hourly spatial distribution map of cyanobacteria blooms on the shoreline of lakes can be drawn by calculating the coverage of cyanobacteria blooms. The technology was successfully used to monitor the cyanobacterial blooms in Chaohu Lake in September 2022. The results showed that, compared to the FCN and U-net models, the DeeplabV3+ model with ResNet-50 network fusion could accurately identify cyanobacteria blooms and delineate the boundary shape of cyanobacteria blooms more clearly. The IOU of cyanobacteria blooms reached 0.72. The RMSE of the predicted and measured cyanobacterial bloom coverage of 43 cameras was 6.65%. The use of multi-threaded technology also ensures that hourly cyanobacterial bloom identification tasks are completed within one hour. Finally, it is proved that this technology can solve the problems of weak timeliness and low accuracy of cyanobacteria bloom monitoring in the lakeshore zone and can provide scientific and technical help for cyanobacteria bloom management personnel. In addition, the technical framework of this study also has certain general adaptive value. For lakes with cyanobacteria as the dominant species, this technology may be directly applied to coastal bloom monitoring; for lakes with non-cyanobacteria as the dominant species, sample data sets need to be remade to train semantic segmentation models.

**Author Contributions:** Conceptualization, Z.W.; Methodology, Z.W.; Software, Z.W.; Validation, Z.W.; Formal Analysis, Z.W.; Resources, Z.W.; Data Curation, Z.W.; Writing—Original Draft Preparation, Z.W.; Writing—Review and Editing, Z.W., C.W., Y.Q. and Y.L.; Visualization, J.W.; Supervision, Y.L.; Funding Acquisition, Y.Q. All authors have read and agreed to the published version of the manuscript.



**Funding:** This work was supported jointly by the Natural Science Foundation of Jiangsu Province (Grant No. BK20201100), the National Natural Science Foundation of China (Grant No. 42101433).

**Institutional Review Board Statement:** Not applicable.

**Informed Consent Statement:** Not applicable.

**Data Availability Statement:** Data are available from the corresponding author upon request.

**Conflicts of Interest:** The authors declare no conflict of interest.

## References

1. Brooks, B.W.; Lazorchak, J.M.; Howard, M.D. Are harmful algal blooms becoming the greatest inland water quality threat to public health and aquatic ecosystems? *Environ. Toxicol. Chem.* **2016**, *35*, 6–13. [[CrossRef](#)] [[PubMed](#)]
2. Amorim, C.A.; do Nascimento Moura, A. Ecological impacts of freshwater algal blooms on water quality, plankton biodiversity, structure, and ecosystem functioning. *Sci. Total Environ.* **2021**, *758*, 143605. [[CrossRef](#)]
3. Wu, T.; Zhu, G.; Zhu, M. Effects of algae proliferation and density current on the vertical distribution of odor compounds in drinking water reservoirs in summer. *Environ. Pollut.* **2021**, *288*, 117683. [[CrossRef](#)]
4. Hou, X.; Feng, L.; Dai, Y. Global mapping reveals increase in lacustrine algal blooms over the past decade. *Nat. Geosci.* **2022**, *15*, 130–134. [[CrossRef](#)]
5. Huang, J.; Zhang, Y.; Huang, Q. When and where to reduce nutrient for controlling harmful algal blooms in large eutrophic lake Chaohu, China? *Ecol. Indic.* **2018**, *89*, 808–817. [[CrossRef](#)]
6. Ma, J.; Jin, S.; Li, J. Spatio-temporal variations and driving forces of harmful algal blooms in Chaohu Lake: A multi-source remote sensing approach. *Remote Sens.* **2021**, *13*, 427. [[CrossRef](#)]
7. Tang, X.; Shen, M.; Duan, H. Temporal and spatial distribution of algal blooms in Lake Chaohu, 2000–2015. *J. Lake Sci.* **2017**, *29*, 276–284.
8. Yuan, J.; Cao, Z.; Shen, M.; Qi, T.; Duan, H. Remote sensed analysis of spatial and temporal variation in algal blooms phenology in Lake Chaohu since 1980s. *J. Lake Sci.* **2022**, *1*, 18.
9. Yoon, H.; Kim, H.C.; Kim, S. Long-term seasonal and temporal changes of hydrogen peroxide from cyanobacteria blooms in fresh waters. *J. Environ. Manag.* **2021**, *298*, 113515. [[CrossRef](#)]
10. Mishra, S.; Stumpf, R.P.; Schaeffer, B.A. Measurement of cyanobacteria blooms magnitude using satellite remote sensing. *Sci. Rep.* **2019**, *9*, 1–17. [[CrossRef](#)] [[PubMed](#)]
11. Shi, K.; Zhang, Y.; Qin, B. Remote sensing of cyanobacteria blooms in inland waters: Present knowledge and future challenges. *Sci. Bull.* **2019**, *64*, 1540–1556. [[CrossRef](#)]
12. Sayers, M.J.; Grimm, A.G.; Shuchman, R.A. Satellite monitoring of harmful algal blooms in the Western Basin of Lake Erie: A 20-year time-series. *J. Great Lakes Res.* **2019**, *45*, 508–521. [[CrossRef](#)]
13. Caballero, I.; Fernández, R.; Escalante, O.M. New capabilities of Sentinel-2A/B satellites combined with in situ data for monitoring small harmful algal blooms in complex coastal waters. *Sci. Rep.* **2020**, *10*, 1–14. [[CrossRef](#)] [[PubMed](#)]
14. Huang, C.; Shi, K.; Yang, H. Satellite observation of hourly dynamic characteristics of algae with Geostationary Ocean Color Imager (GOCI) data in Lake Taihu. *Remote Sens. Environ.* **2015**, *159*, 278–287. [[CrossRef](#)]
15. Zhang, Y.; Zhang, Y.; Li, N.; Sun, X.; Wang, W.; Qin, B.; Zhu, G. Capturing the rapid intra-day change of cyanobacteria blooms by land-based hyperspectral remote sensing in Lake Taihu. *J. Lake Sci.* **2021**, *33*, 1951–1960.
16. Ma, T.; Xiao, P.; Zhang, X.; Duan, H.; Qiu, Y. Real-time monitoring of cyanobacteria blooms dynamics around Lake Chaohu based on video surveillance images. *J. Lake Sci.* **2022**, *34*, 1840–1853.
17. Jiang, F.; Grigorev, A.; Rho, S. Medical image semantic segmentation based on deep learning. *Neural Comput. Appl.* **2018**, *29*, 1257–1265. [[CrossRef](#)]
18. Abdar, M.; Pourpanah, F.; Hussain, S. A review of uncertainty quantification in deep learning: Techniques, applications and challenges. *Inf. Fusion* **2021**, *76*, 243–297.
19. Long, J.; Shelhamer, E.; Darrell, T. Fully convolutional networks for semantic segmentation. In Proceedings of the IEEE Conference on Computer Vision and Pattern Recognition, Boston, MA, USA, 7–12 June 2015; pp. 3431–3440.
20. Ronneberger, O.; Fischer, P.; Brox, T. U-net: Convolutional networks for biomedical image segmentation. In Proceedings of the International Conference on Medical Image Computing and Computer-Assisted Intervention, Munich, Germany, 5–9 October 2015; Springer: Cham, Switzerland, 2015; pp. 234–241.
21. Son, S.; Lee, S.-H.; Bae, J.; Ryu, M.; Lee, D.; Park, S.-R.; Seo, D.; Kim, J. Land-Cover-Change Detection with Aerial Orthoimagery Using SegNet-Based Semantic Segmentation in Namyangju City, South Korea. *Sustainability* **2022**, *14*, 12321. [[CrossRef](#)]
22. Zhao, H.; Shi, J.; Qi, X. Pyramid scene parsing network. In Proceedings of the IEEE Conference on Computer Vision and Pattern Recognition, Honolulu, HI, USA, 21–26 July 2017; pp. 2881–2890.
23. Chen, L.C.; Zhu, Y.; Papandreou, G. Encoder-decoder with atrous separable convolution for semantic image segmentation. In Proceedings of the European Conference on Computer Vision, Munich, Germany, 8–14 September 2018; pp. 801–818.
24. Matin, M.M.H.; Khatun, A.; Moazzam, M.G.; Uddin, M.S. An efficient disease detection technique of rice leaf using AlexNet. *J. Comput. Commun.* **2020**, *8*, 49. [[CrossRef](#)]



25. Qian, M.; Li, Y.; Zhao, Y.; Yu, X. Prior Knowledge-Based Deep Convolutional Neural Networks for Fine Classification of Land Covers in Surface Mining Landscapes. *Sustainability* **2022**, *14*, 12563. [[CrossRef](#)]
26. He, K.; Zhang, X.; Ren, S. Deep residual learning for image recognition. In Proceedings of the IEEE Conference on Computer Vision and Pattern Recognition, Las Vegas, NV, USA, 27–30 June 2016; pp. 770–778.
27. Al-Jubouri, H.A.; Mahmmud, S.M. A comparative analysis of automatic deep neural networks for image retrieval. *TELKOMNIKA Telecommun. Comput. Electron. Control* **2021**, *19*, 858–871. [[CrossRef](#)]
28. Theckedath, D.; Sedamkar, R.R. Detecting affect states using VGG16, ResNet50 and SE-ResNet50 networks. *SN Comput. Sci.* **2020**, *1*, 1–7. [[CrossRef](#)]
29. Takisawa, N.; Yazaki, S.; Ishihata, H. Distributed deep learning of ResNet50 and VGG16 with pipeline parallelism. In Proceedings of the 2020 Eighth International Symposium on Computing and Networking Workshops (CANDARW), Naha, Japan, 24–27 November 2020; IEEE: Piscataway, NJ, USA, 2020; pp. 130–136.
30. Wang, X.; Zhang, M.; Yin, J. Composition and influential factors of phytoplankton function groups in Lake Chaohu. *J. Lake Sci.* **2018**, *30*, 431–440.
31. Zhang, M.; Kong, F. The process, spatial and temporal distributions and mitigation strategies of the eutrophication of Lake Chaohu (1984–2013). *J. Lake Sci.* **2015**, *27*, 791–798.
32. Guo, H.; Liu, H.; Lyu, H. Is there any difference on cyanobacteria blooms patterns between Lake Chaohu and Lake Taihu over the last 20 years? *Environ. Sci. Pollut. Res.* **2022**, *29*, 40941–40953. [[CrossRef](#)] [[PubMed](#)]
33. Han, S.H.; Lee, K.Y. Implementation of image classification CNN using multi thread GPU. In Proceedings of the International SoC Design Conference, Seoul, Republic of Korea, 5–8 November 2017; IEEE: Piscataway, NJ, USA, 2017; pp. 296–297.
34. Lyu, K.; Li, Y.; Zhang, Z. Attention-aware multi-task convolutional neural networks. *IEEE Trans. Image Process.* **2019**, *29*, 1867–1878. [[CrossRef](#)]
35. Kim, C.G. An implementation and performance evaluation of fast web crawler with Python. *J. Semicond. Disp. Technol.* **2019**, *18*, 140–143.
36. Mascarenhas, S.; Agarwal, M. A comparison between VGG16, VGG19 and ResNet50 architecture frameworks for Image Classification. In Proceedings of the 2021 International Conference on Disruptive Technologies for Multi-Disciplinary Research and Applications, Bengaluru, India, 19–21 November 2021; IEEE: Piscataway, NJ, USA, 2021; Volume 1, pp. 96–99.
37. Jafari, N.H.; Li, X.; Chen, Q.; Le, C.Y.; Betzer, L.P.; Liang, Y. Real-time water level monitoring using live cameras and computer vision techniques. *Comput. Geosci.* **2021**, *147*, 104642. [[CrossRef](#)]
38. An, S.; Rui, X.A. High-Precision Water Body Extraction Method Based on Improved Lightweight U-Net. *Remote Sens.* **2022**, *14*, 4127. [[CrossRef](#)]
39. Fu, J.; Yi, X.; Wang, G.; Mo, L.; Wu, P.; Kapula, K.E. Research on Ground Object Classification Method of High Resolution Remote-Sensing Images Based on Improved DeeplabV3+. *Sensors* **2022**, *22*, 7477. [[CrossRef](#)] [[PubMed](#)]
40. Wang, Z.; Wang, J.; Yang, K.; Wang, L.; Su, F.; Chen, X. Semantic segmentation of high-resolution remote sensing images based on a class feature attention mechanism fused with Deeplabv3+. *Comput. Geosci.* **2022**, *158*, 104969. [[CrossRef](#)]
41. Verma, U.; Chauhan, A.; Manohara Pai, M.M.; Pai, R. DeepRivWidth: Deep learning based semantic segmentation approach for river identification and width measurement in SAR images of Coastal Karnataka. *Comput. Geosci.* **2021**, *154*, 104805. [[CrossRef](#)]
42. Wynne, T.T.; Mishra, S.; Meredith, A.; Litaker, R.W.; Stumpf, R.P. Intercalibration of MERIS, MODIS, and OLCI Satellite Imagers for Construction of Past, Present, and Future Cyanobacterial Biomass Time Series. *Remote Sens.* **2021**, *13*, 2305. [[CrossRef](#)]
43. Castagna, A.; Simis, S.; Dierssen, H.; Vanhellemont, Q.; Sabbe, K.; Vyverman, W. Extending Landsat 8: Retrieval of an Orange contra-Band for Inland Water Quality Applications. *Remote Sens.* **2020**, *12*, 637. [[CrossRef](#)]
44. Yan, K.; Li, J.; Zhao, H.; Wang, C.; Hong, D.; Du, Y.; Mu, Y.; Tian, B.; Xie, Y.; Yin, Z.; et al. Deep Learning-Based Automatic Extraction of Cyanobacterial Blooms from Sentinel-2 MSI Satellite Data. *Remote Sens.* **2022**, *14*, 4763. [[CrossRef](#)]

**Disclaimer/Publisher’s Note:** The statements, opinions and data contained in all publications are solely those of the individual author(s) and contributor(s) and not of MDPI and/or the editor(s). MDPI and/or the editor(s) disclaim responsibility for any injury to people or property resulting from any ideas, methods, instructions or products referred to in the content.